Experimental and theoretical study of the vapor-cell Zeeman optical trap

K. Lindquist, M. Stephens, and C. Wieman
Joint Institute for Laboratory Astrophysics and Physics Department, University of Colorado, Boulder, Colorado 80309-0440
(Received 24 April 1992)

We present an experimental study of the number and density of trapped atoms in a vapor-cell Zeeman optical trap. We have investigated how the number (and therefore the capture rate) and density change with the trapping laser's beam diameter, intensity, and detuning and with the magnetic-field gradient of the trap. We have developed a quasi-one-dimensional numerical model that accurately predicts the number of trapped atoms for all conditions. We also have investigated chirping the laser frequency and trapping with broadband light, neither of which increase the number of trapped atoms.

PACS number(s): 32.80.Pj, 42.50.Vk

I. INTRODUCTION

Much recent progress in optical trapping of neutral atoms has been driven by the appeal of large samples of cold, dense atoms [1]. Such samples will be useful for high-resolution spectroscopy [2,3], collision measurements [4–7], and time and frequency standards [1,8,9]. They will also be useful for studying rare, radioactive isotopes in β decay and atomic parity-nonconservation experiments [10,11]. Additionally, optical traps can be used to load magnetic traps in an attempt to see Bose condensation [12] and for other fundamental physics experiments.

The vapor-cell Zeeman-shift optical trap (ZOT), described below, produces these cold samples in a simple and inexpensive manner. However, despite the growing popularity of the vapor-cell trap, there has never been a detailed study of how to optimize the number and density of trapped atoms. These characteristics are important for most applications.

We have determined how the number and density of trapped atoms vary with the laser beam sizes, laser intensities, laser detunings, and magnetic-field gradients. We have developed a simple model of the slowing that agrees well with the measurements of the number of trapped atoms. We have also explored two techniques for increasing the capture rate of the trap: frequency chirping [13] and bandwidth broadening [14] of the trapping light. Neither technique was successful.

In what follows we first explain our experimental setup and measurements in Sec. II, and then present our data on the number of atoms in Sec. III. In Sec. IV we describe the model that explains these results, and compare its predictions to our data. In the course of this work, we learned of the results of Gibble, Kasapi, and Chu [15] and have included them in our comparison. In Sec. V we discuss the frequency chirping experiments and calculations and finally, in Sec. VI, we present measurements of the density of trapped atoms.

II. EXPERIMENTAL APPARATUS

Our apparatus is similar to that of Monroe *et al.* [16]. The ZOT is a spontaneous-force optical trap consisting of a spatially varying magnetic field and three orthogonal pairs of counterpropagating laser beams of opposite helicity. The laser beams intersect in a fused-silica cell that is filled with a 10^{-8}-Torr room-temperature cesium vapor. The frequency of the light is slightly below the 852-nm cesium D_2 transition. When Doppler shifts induce absorption imbalances between opposing beams, the resulting difference in radiation pressures slows down atoms in the low-velocity tail of the Maxwell-Boltzmann distribution. A quadrupole magnetic field induces a position-dependent shift in the Zeeman levels of the slowed atoms, which causes a position-dependent radiation pressure, thus trapping the slowed atoms [17].

The vapor cell is a 9-cm-long, 2.5-cm-diam cylinder with windows on each end. Two tubes each 4.5 cm long and 2.5 cm in diameter intersect the cylinder at right angles to form a six-way cross. Two smaller tubes are attached to the main cylinder. One is a "cold finger" containing a reservoir of cesium, whose temperature determines the vapor pressure in the cell. The second tube leads to a 2-liter/s ion pump, which removes any residual gas (mostly helium) that diffuses through the walls of the cell [16].

The trapping beams come from an STC Optical Devices diode laser. We tune the laser frequency and reduce the laser linewidth to much less than 1 MHz with optical feedback from a diffraction grating [18]. The laser frequency is locked to the side of the $6S_{1/2}$, $F=4\rightarrow 6P_{3/2}$, $F=5$ cycling transition in cesium using the signal from a saturated-absorption spectrometer. The laser's output is split into three circularly polarized beams of 5 mW each. These beams enter and exit the cell along three orthogonal axes, pass through quarter-wave plates, and then are retroreflected. The trapping beams are focused to compensate for intensity losses from the cell windows so that the incident and reflected beams have the same intensity. A 20-mW beam from a second diode laser, frequency locked to the $6S_{1/2}$, $F=3\rightarrow 6P_{3/2}$, $F=4$ transition, overlaps one of the trapping beams. This "hyperfine pumping" laser prevents the atoms from accumulating in the $F=3$ ground state.

The quadrupole magnetic field is provided by a pair of coils with counterpropagating currents. The coil spacing is equal to the 5 cm diam of the coils. This "Maxwell

 ©1992 The American Physical Society

configuration" provides a very linear field gradient in all three directions, which simplifies the comparison of the model to the experiment. Three additional, orthogonal shim coils cancel stray fields in the region of the trap.

We measure the number of trapped atoms by imaging the fluorescence of the cloud onto a photodiode, which gives us the rate at which protons are scattered by the cloud. We assume [5,19] that the number of atoms is proportional to the total fluorescence, with a proportionality constant given by the power-broadened scattering rate, which depends on the laser's detuning and intensity.

The following procedure is used to ensure that the relative uncertainty between measurements is significantly smaller than our uncertainty for the absolute number of atoms. First, we let the trap reach equilibrium at the detuning and magnetic field of interest, then we quickly shift the laser frequency to a standard detuning of -1.5Γ and turn off the magnetic field. Here Γ is the 5-MHz natural linewidth of the transition, and the detuning is defined by $\Delta=\nu_{\text{laser}}-\nu_{\text{atom}}$. We record the fluorescence during the next 10 ms. Turning off the magnetic field eliminates the $\sim 10\%$ effects of the magnetic field on the scattering rate. The fluorescence from the cloud takes about 0.4 s to change after the adjustments in detuning and magnetic field, so this provides an accurate measurement of the number of trapped atoms.

Varying the trap parameters to determine how they affect the number of trapped atoms is straightforward. We change the trapping beam intensities by placing neutral density filters in the beam before it is split into three parts. To change the beam diameter, we replace the lenses in our beam-expansion telescope. The magnetic field can be varied by adjusting the current in the Maxwell coils. Laser detuning is controlled by a variable set point in the frequency locking circuitry.

To obtain the density of the cloud of trapped atoms, we measure both the volume of the cloud and the number of atoms in the trap. To measure the volume, we image the cloud from the top and from the side with two charge-coupled device video cameras. The horizontal and vertical axes of the camera images coincide approximately with the semimajor axes (a,b,c) of the ellipsoidal cloud of trapped atoms, allowing us to calculate the volume of the cloud as $V=\frac{4}{3}\pi abc$. The process used to determine the number of pixels covered by the 1–5-mm clouds is described in Ref. [20]. The resolution is 0.1–0.2 mm, depending on the camera and on the dimension (horizontal or vertical) involved; care must be taken to avoid saturating the cameras.

These number and density measurements are quite sensitive to the alignment of the trapping beams, so the beams are carefully aligned to give ellipsoidal cloud shapes. As a check on our alignment, we turn off the magnetic field, then watch the atoms diffuse out of the laser-beam intersection region. Atoms from well-aligned traps diffuse away slowly and isotropically.

III. DATA—NUMBER OF ATOMS

Figures 1–3 illustrate how the number of trapped atoms depends on various parameters. Only part of our data is shown, to indicate the significant trends. We find that the number of atoms is quite sensitive to alignment. After major realignment of the trap, our numbers are reproducible to within 20%, whereas measurements made when no realignment is necessary are reproducible to better than 10%.

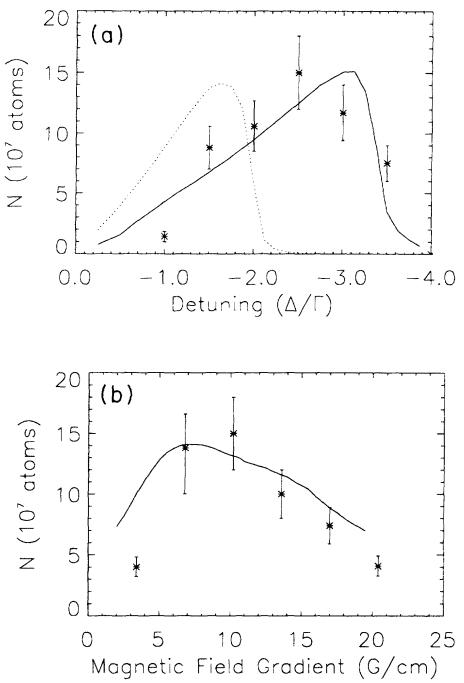

FIG. 1. (a) The number of trapped atoms vs the laser detuning at a constant magnetic-field gradient of 11 G/cm. (b) The number of trapped atoms vs the magnetic-field gradient, at a detuning of -2.5Γ. The beam diameter for both (a) and (b) is 1.9 cm and the intensity in each of the six beams is 1.6 mW/cm^2. The asterisks are our data, and the solid line shows the predictions of the model that includes the magnetic field. The dashed line is the prediction of the two-level model.

Figure 1(a) shows how the number of atoms depends on detuning at a fixed magnetic-field gradient; Fig. 1(b)

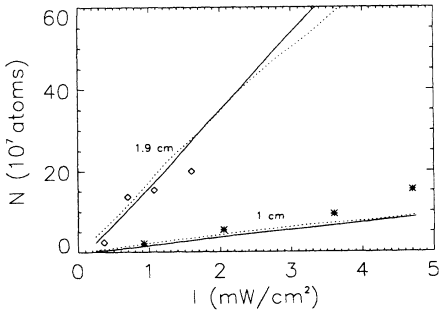

FIG. 2. The number of trapped atoms vs intensity at constant beam diameter: asterisks are our data for a trap with a 1-cm beam diameter, diamonds are for a 1.9-cm beam. Each data point was taken at the optimum detuning and optimum magnetic-field gradient for the given beam size and intensity. The solid lines represent the number of atoms predicted by the model that includes the magnetic field. The dotted line shows the predictions of the two-level model.

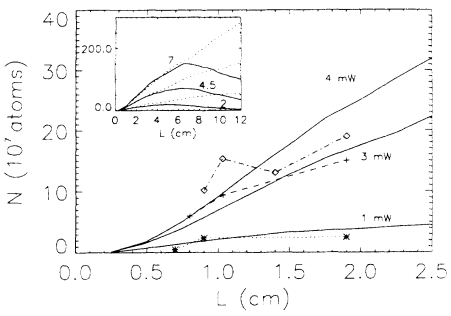

FIG. 3. Number of atoms vs $1/e$ beam diameter, L, when the total power in each beam is held as constant as possible. Asterisks indicate data for powers from 0.9 to 1.2 mW per beam, crosses are 2.7–3.2 mW per beam, diamonds are 4–4.5 mW per beam. The power variation in each trace is responsible for some of the scatter in the data. Each data point was taken at the optimum detuning and optimum magnetic-field gradient for the beam size and power. The solid lines indicate the number of atoms predicted by the model with the magnetic field. The inset shows, on a condensed scale, the predicted number of atoms as a function of beam size for three powers: 2, 4.5, and 7 mW per beam. Solid lines represent predictions made by the model when the magnetic field is included; dotted lines represent predictions made by the two-level model.

shows how the number of atoms depends on the magnetic-field gradient at a fixed detuning. For each beam size and beam intensity, there is an optimum detuning and an optimum magnetic field; as the detuning is increased, the optimum magnetic-field gradient for that detuning increases.

Figure 2 shows that as the intensity is increased for a fixed beam diameter, the number of atoms increases approximately linearly. This applies when the detuning and magnetic field are optimized for each intensity, and the intensity is not too high.

We also found that, for a fixed power, a larger beam diameter L always resulted in a larger number of trapped atoms (see Fig. 3) despite the corresponding decrease in the intensity of the trapping beams to well below the saturation intensity of the optical transition. This was true over the entire range of sizes we were able to study, but, as discussed in Sec. IV, we expect this to fail for very large L.

Finally, as L increases while the peak intensity is held constant, the number of atoms increases very rapidly. This measurement is particularly alignment sensitive; therefore, the uncertainty in our data is quite large.

As shown in Table I, for the beam sizes and intensities that are available with this apparatus, the detunings that provide the maximum number of atoms are in a small interval around -2.25Γ and the optimum magnetic-field gradients along the axis of the coils are between 10 and 15 G/cm. This is in agreement with previous work [15,16]. As can be seen from the table, the optimum values are slowly increasing functions of both intensity and beam diameter. This is reasonable: a larger beam size creates a longer stopping region, which means that faster atoms can be stopped. This results in an increase in the optimum detuning since faster atoms have larger Doppler shifts.

To determine whether any important slowing takes place outside the region where the three trapping beams overlap, we varied the volume illuminated by the hyperfine repumping ($F=3\rightarrow F'=4$) laser. We observed that the same number of atoms were trapped whether the repumping light overlapped just one of the trapping beams, or overlapped all three trapping beams. Since repumping is necessary for slowing, we conclude that any slowing that takes place outside the three-beam overlap region does not contribute to the number of atoms trapped. Consequently, the models described in the next section consider the slowing forces only in the overlap region.

IV. THEORETICAL MODELS OF THE CAPTURE PROCESS

In this section we present two different models of the capture process and compare them with the data. The first model is a very simple calculation which treats the atom as a two-level system and ignores the magnetic field and the Gaussian profile of the beam. While it does not match all the observations, it is quite useful in that it does predict most of the general trends quite accurately. This allows one to predict capture rates for most situations reasonably well with just a few lines of code on any personal computer. The second model agrees with all of our observations, as well as those made by Gibble, Kasapi, and Chu [15] at larger beam sizes and higher intensities than attainable in our experiment. Although this model is somewhat more elaborate, it is still surprisingly simple.

Monroe, Robinson, and Wieman [8] have shown that the steady-state number of atoms in the trap is given by

TABLE I. The optimum detunings and magnetic-field gradients predicted by the model are compared to the measured optima. The number of atoms measured in each case and the predicted average capture velocity are also shown. The last line is data of Gibble, Kasapi, and Chu [15].

Beam size	Intensity	Δ (units of Γ)		Field gradient (G/cm)		N	v_c (average)
(cm)	(mW/cm^2)	Opt.	Pred.	Opt.	Pred.	(units of 10^8)	(m/s)
0.9	1.9	−2.0	−2.5	10	18	0.3	11
0.9	7.7	−2.5	−3.0	12	18	1.2	16
1.0	4.0	−2.5	−3.0	13	18	1.5	14
1.9	1.6	−2.5	−3.0	10	12	2.0	15
4.0	22.0	−4.0	−6.5	7.7	9.0	360.0	36

$$N = R\tau_{\text{trap}} = 0.1\frac{A}{\sigma}\left[\frac{v_c}{v_{\text{thermal}}}\right]^4, \quad (1)$$

where R is the capture rate and $1/\tau_{\text{trap}} = n_0\sigma v_{\text{rms}}$ is the loss rate due to collisions between trapped atoms and atoms in the room-temperature Cs background gas. The cross section σ for these collisions [16] is 2×10^{-13} cm^2, $n_0 = 10^8$/cm^3 is the density of the background gas, and $v_{\text{rms}} = 236$ m/s is the root-mean-square velocity. The capture rate involves the surface area A of the trap volume, and the ratio v_c/v_{thermal}, where v_c is the maximum velocity an atom can have and be captured, and $v_{\text{thermal}} = 193$ m/s is the average velocity of the background gas. We assume that all atoms entering the trapping region at speeds below v_c will be trapped. Because τ depends only on the characteristics of the background gas, which are constant, a change in the number of atoms in the trap is equivalent to a change in the capture rate R. Thus, if one is interested in using the trap as a pulsed source of cold atoms, the production rate can be calculated from our values for N using Eq. (1). This equation neglects the contribution of intratrap collisions to the loss rate of the trap [5]. For the densities of background vapor and trapped atoms at which we operated, this contribution is relatively small and thus does not affect most of the comparisons we make between our model and our data. In our discussion, we point out the few cases where the contribution may be significant.

Equation (1) shows that to predict the number of trapped atoms we need to calculate only v_c and A. We find v_c by computing the one-dimensional slowing forces on an atom in the trapping region. These forces are nearly the same along the three axes which allows us to consider only atoms moving in the x direction, but the calculated v_c will be valid for all directions. The slowing force for an atom moving in the $+x$ direction is proportional to the difference between the numbers of photons scattered from the two beams propagating along the x axis. In our first model we make the great simplification of treating the atom as a two-level system in one dimension, thus ignoring the magnetic field and the Gaussian intensity profile of the laser beams. The radiation-pressure force can then be written

$$F = \frac{h\nu}{2\tau_{\text{atom}}c}\beta\left[\frac{1}{1+\beta+4\left[\frac{\Delta}{\Gamma}-\frac{kv}{2\pi\Gamma}\right]^2} - \frac{1}{1+\beta+4\left[\frac{\Delta}{\Gamma}+\frac{kv}{2\pi\Gamma}\right]^2}\right], \quad (2)$$

where $\beta = I/I_{\text{sat}}$ is the saturation parameter for one beam, I is the intensity in each beam, and $I_{\text{sat}} = 2.7$ mW/cm^2; $k = 7400$ cm^{-1} is the wave number of the trapping light; $\Delta = \nu_{\text{laser}} - \nu_{\text{atom}}$ is the detuning of the laser, $\nu_{\text{atom}} = 3.52\times10^{14}$ Hz, and τ_{atom} is the 31-ns excited-state lifetime. We neglect the saturation effects from the orthogonal trapping beams because during nearly all of the time the atom is being slowed its velocity is high enough that the beam in the negative x direction is Doppler shifted closer to resonance with the atoms than the other beams, and hence dominates the excitation.

To find the maximum capture velocity, the equation of motion is solved numerically with the constraint that the atom must be stopped ($v < 10$ cm/s) by the time it has traversed the trapping region. The length of the trapping region is defined to be the $1/e$ diameter of the trapping beam's Gaussian intensity profile (we do not include the Gaussian profile anywhere else in the two-level model). Once v_c has been found, the number of atoms trapped is calculated from Eq. (1). To determine the surface area of the trapping region, we assume that it is spherical, with a diameter equal to the beam diameter, $A = \pi L^2$. This very simple model predicts values for the number of atoms that are approximately 0.3 of those observed (a 35% error in v_c). To better illustrate how well the model predicts general trends, we have normalized all the predicted values by dividing by 0.3.

In Figs. 2–4 we compare the normalized predictions with observations. Note that this extremely simple model predicts most general trends in the capture rates remarkably well; the two areas where it fails most conspicuously are in predicting the optimum detuning, and of course the dependence on magnetic field. The error in the detuning dependence is reflected in Fig. 1(a) and in the low-intensity part of Fig. 4. The detuning was kept constant at -4Γ throughout the measurements displayed in Fig. 4. This is only slightly higher than the actual optimum detuning for low intensities, but substantially larger than -1.5Γ, which is the optimum predicted by this model. The predicted number of atoms is lower when the model detuning is specified to be -4Γ. If in-

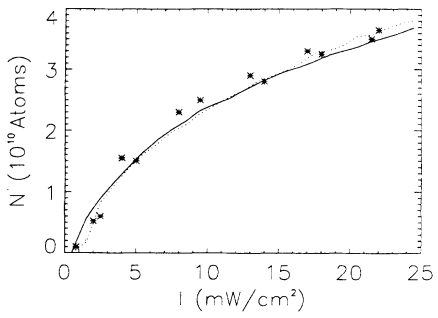

FIG. 4. The results or our models are compared with the data of Gibble, Kasapi, and Chu [15]. As in Fig. 2, the numbers of atoms trapped are shown as a function of intensity, but rather than optimizing the detuning and the magnetic field at each point (as in Fig. 2), the detuning is kept constant at -4Γ and the magnetic field is kept constant at 7.7 G/cm, which are the conditions specified in Ref. [15]. The beam diameter is 4 cm. Asterisks are data from Gibble, Kasapi, and Chu, the solid line shows the predictions of the model that includes the magnetic field, the dotted line illustrates predictions of our two-level model. The rolloff at high intensities is due to saturation of the optical transition. For both models the values for the numbers of atoms were normalized to 3.6×10^{10} atoms at 22 mW/cm^2. The normalization factor was 3.2 for the magnetic-field model, and 4.2 for the two-level model.

stead of taking the predicted number at a fixed detuning, we take the number at the optimum detuning, as in Fig. 2, then there is much better agreement. In fact, with optimized detuning, this model matches the experimental intensity dependence shown in Fig. 4 quite closely. In summary, this one-dimensional two-level model makes it possible to easily estimate how capture rates will scale with the laser-beam diameter and intensity, or any of the other factors that are included in Eq. (2). Of course it cannot predict the dependence on the magnetic-field gradient, such as shown in Fig. 1, and it is off by about 60% for the absolute number of trapped atoms.

To overcome these limitations, we carried out a more elaborate calculation which includes the magnetic field and the multiple m levels of the atom. The quadrupole magnetic field causes position-dependent splitting of the Zeeman levels of the Cs atom. There is a corresponding shift in the frequency of the optical transition:

$$\delta_B = \frac{\mu_B}{h} B (g_{F'=5} m_{F'} - g_{F=4} m_F) , \tag{3}$$

where B is the magnitude of the magnetic field, $g_{F=4}=0.25$ and $g_{F'=5}=0.4$ are Landé g factors, μ_B is the Bohr magneton, and h is Planck's constant. This position-dependent frequency shift results in a position-dependent change in the effective laser detuning. Therefore, the slowing force is a function of the position of the atom as well as its velocity.

The slowing force in the x direction is a function not only of x, but also of y and z. If the atom that is being slowed enters the trapping region displaced from the x axis (but still with velocity in the $+x$ direction only), it moves through a quadrupole magnetic field that has x, y, and z components (Fig. 5). As a result, the circularly polarized light propagating in the x direction will drive $\Delta m = \pm 1$ and 0 transitions (in the basis defined by the magnetic field). As discussed below, this reduces the effect of the magnetic field on the slowing process. The substantial and changing magnetic field acting upon the atom as it moves through the trapping region also tends to equalize the populations of the different m levels. We believe this is the reason our model, which assumes no optical pumping or other ground-state coherences, is successful.

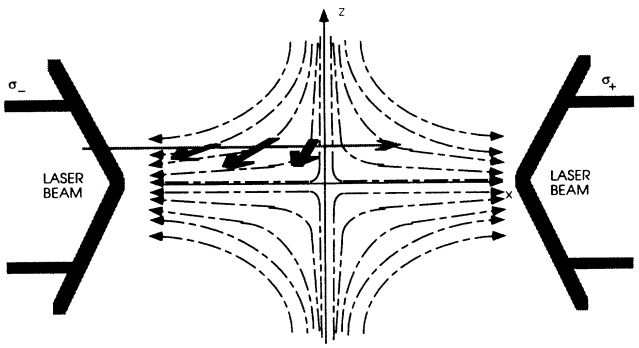

FIG. 5. Spatial variation of the magnetic field in the trap. The grey arrow shows one possible path of an atom through the trap. The dark, black arrows indicate the direction of the magnetic field at several points along the atom's path.

Because of this important three-dimensional character of the magnetic field, we must calculate v_c in the x direction as a function of the z and y coordinates of the atom when it enters the trapping volume. The $(v_c/v_{\text{thermal}})^4$ in Eq. (1) must now be replaced by an average over the beam's cross section, so that Eq. (1) becomes

$$N = 0.1 \sum_{y=-L/2}^{y=L/2} \sum_{z=-L/2}^{z=L/2} \left[\frac{v_c(y,z)}{v_{\text{thermal}}} \right]^4 \frac{\Delta y \Delta z}{\sigma} . \tag{4}$$

To find the position-dependent slowing force, the angular momenta of the trapping lasers were rotated into the basis of the magnetic field at each position. Then the total stopping force was calculated by summing over the force produced by each Δm transition:

$$F = \sum_{\Delta m=-1}^{\Delta m=+1} \sum_{m_F=-5}^{m_F=+5} P_{\text{light}}(\Delta m) P_{\text{trans}}(\Delta m, m_F) \frac{I(y,z)}{I_{\text{sat}}(\Delta m, m_F)} \times \left[\frac{1}{1+\frac{I(y,z)}{I_{\text{sat}}(\Delta m, m_F)}+4\left[\frac{\Delta}{\Gamma}-\frac{\delta_B}{\Gamma}-\frac{kv}{2\pi\Gamma}\right]^2} - \frac{1}{1+\frac{I(y,z)}{I_{\text{sat}}(\Delta m, m_F)}+4\left[\frac{\Delta}{\Gamma}-\frac{\delta_B}{\Gamma}+\frac{kv}{2\pi\Gamma}\right]^2} \right] , \tag{5}$$

where $I(y,z)=I_0 \exp[-4(y^2+z^2)/L^2]$ is the intensity of a single beam, and the saturation parameter I_{sat} depends on the transition and the initial m level. Note that the Gaussian profile of the beam is now explicitly included in the model. $P_{\text{light}}(\Delta m)$ is the fraction of the light that drives $\Delta m = 1$, 0, or -1 transitions and $P_{\text{trans}}(\Delta m, m_F)$ is the m_F to $m_{F'}$ transition probability. This now models the trapping volume as a cube with side L, rather than as a sphere. With this model, the absolute number of atoms is predicted more accurately, as one might expect. The normalization factor to best fit all our data with the model is 1.6, which is well within the uncertainty for the value of σ. As mentioned above, we use a different normalization factor when we make comparisons with the data in Gibble, Kasapi, and Chu [15].

In addition to the approximations already noted, this model neglects the effect of saturation on the distribution of atomic populations. For large-m_F sublevels of the

ground state, the transition probability for one of the three Δm transitions (either $\Delta m=+1$ or -1) is much greater than the transition probability for the other two. If the intensity is high, the strong transition will saturate before the others, reducing the ground-state population and therefore reducing the probability that the other Δm transitions will be excited. We have tested the importance of this effect by introducing a correction factor in Eq. (5) to approximate the effect of the saturation. We found that it did not significantly affect the results. We also neglect the effects of the orthogonal beams, as in the previous model.

The results of our normalized model, and comparisons with our data and those of Gibble, Kasapi, and Chu [15], can be seen in Figs. 1–4 where the agreement appears to be quite good. One difference from the previous model [see Fig. 1(b)] is in the predicted number of atoms, which is larger than the measured values for low fields. The reason for this difference is that the *slowing* of the atoms is being modeled—not the trapping. When there is no magnetic field, and therefore no ZOT, atoms are still being slowed. There is still a maximum capture velocity; therefore at zero magnetic field this model will erroneously predict some number of trapped atoms. The only other significant discrepancy is between the predicted and measured optimum detunings (Table I), particularly at the larger beam size and intensity used by Gibble, Kasapi, and Chu [15]. The increase in the loss rate due to light-induced intratrap collisions, which we have neglected, may be large enough to affect the number of trapped atoms for the parameters used by Gibble, Kasapi, and Chu. Also the uncertainty in the detuning data is not clear, so the discrepancy may be smaller than it appears.

Our model predicts that as L is increased while the intensity is held constant, the number of trapped atoms increases as $L^{3.6}$ (see Fig. 6). This is consistent with our measurements, and with the exponent of 3.65 measured by Gibble, Kasapi, and Chu [15]. At small beam sizes and high intensities, the number of atoms is not proportional to $L^{3.6}$, because the number of atoms that can be trapped is limited by the available stopping distance rather than by intensity. The beam size at which the number of atoms begins to follow the relationship $N\sim L^{3.6}$ depends on the intensity, as shown.

The major difference, besides the normalization, between the predictions made by this model and the two-level model can be seen in the inset of Fig. 3. This model predicts that there is a large optimum beam size for a given power. This optimum is to be expected: for very large beam sizes the Zeeman shift at the edge of the trap is large enough to interfere with the slowing of the atoms, even with very small magnetic-field gradients. We find that the optimum magnetic field for the *slowing* is zero. However, since in practice a magnetic field is required to obtain a trap, in the simulations the magnetic-field gradient was not permitted to drop below 3 G/cm along the axis of the coils. This gradient limits the size over which the advantage of a long stopping region overcomes the disadvantage of lower intensity.

An interesting prediction of this model is that if the intensities of the three trapping beams are equal, the capture velocity along the longitudinal axis of the magnetic-field coils will be slightly smaller than that along the radial axes because the magnetic-field gradient along the axis of the coils is twice that of either radial gradient. For a constant total power in the six beams, our model predicts that a slight (10–15 %) increase in the number of atoms trapped is achieved by increasing the power in the trapping beams along the longitudinal axis by about 20%. This was tested by adjusting the powers in the different beams, which produced an increase in the number of trapped atoms of just the size predicted.

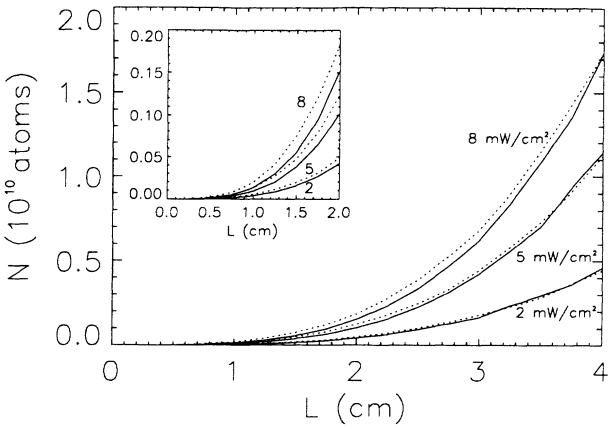

FIG. 6. Predicted dependence of the number of atoms on the trapping beam size for beams of constant intensities. Predictions are shown for beams with intensities of 2, 5, and 8 mW/cm^2. The solid lines are predictions of the model that includes the magnetic field; dotted lines shown predictions of the model that does not include the magnetic field (normalized to match predictions of the other model at a 4-cm beam size). The detuning and magnetic field were optimized at each point. The inset shows the same predictions for smaller beam sizes.

Our results clarify a question that has come out of previous calculations. Metcalf [21] had predicted capture velocities for metastable helium that depended strongly on magnetic field. When scaled to cesium, these velocities were far larger than what has been observed. We believe this discrepancy was the result of considering the magnetic field only along the central axis of the laser beams where it is parallel to the wave vector. As we discuss above, most of the atoms enter the trap off axis, where the magnetic field and the wave vector of the laser beam are not parallel. This allows $\Delta m=+1$, -1, and 0 transitions to be excited. The net effect is that the magnetic field has far less influence on the slowing than is calculated when one considers only the on-axis case, as was done in Ref. [21].

V. CHIRPING

We have also explored the possibility of increasing the trapping rate by chirping the laser frequency. Frequency chirping (sweeping the laser frequency repeatedly from large to small detunings) has been used with success to slow atomic beams [22,23], and it has been suggested that the technique would also allow a greater capture rate in a vapor-cell trap [13]. The reasoning is that to increase the

capture velocity, one must increase the laser's detuning to adjust for the larger Doppler shifts seen by faster atoms. One then sweeps the laser's frequency to keep it in resonance with the atoms as they slow down. We have studied this idea experimentally and compared our measurements with the predictions of the model described above. The number of atoms in the trap was measured while the laser was being linearly chirped. The data shown in Fig. 7 were taken with a chirp period of 1 ms, which both experiment and theory showed to be the optimum. The chirp period could be varied by about a factor of 2 without substantial change in the number of trapped atoms. The number of trapped atoms is maximized when the starting detuning is about -4Γ, and never exceeds the number obtained in the unchirped case.

In principle, the laser's frequency chirp should compensate not only for Doppler shifts, but also for Zeeman shifts caused by the spatially varying magnetic field. This means that a linear frequency chirp is not the ideal time dependence. However, since the Zeeman shifts are small compared to the Doppler shifts it should still be close to optimum.

Our calculations again gave values quite similar to the experimental values, and made it clear why chirping does not work. Since the atoms in the trap are captured from a background gas of cesium in the cell, not all the atoms entering the slowing region will do so when the laser is at the point of farthest detuning. Some of the atoms will enter the slowing region "out of phase" with the laser's frequency chirp. The number of trapped atoms is therefore given by

$$N = 0.1\frac{A}{\sigma}\frac{\int_0^{\tau_{\text{chirp}}} \frac{v_c^4(\tau)d\tau}{v_{\text{thermal}}^4}}{\int_0^{\tau_{\text{chirp}}} d\tau} . \tag{6}$$

While a large capture velocity is obtained for atoms that enter the trapping volume at just the right phase of the chirping cycle, this is more than offset by the reduced capture velocities during out-of-phase parts of the chirp cycle.

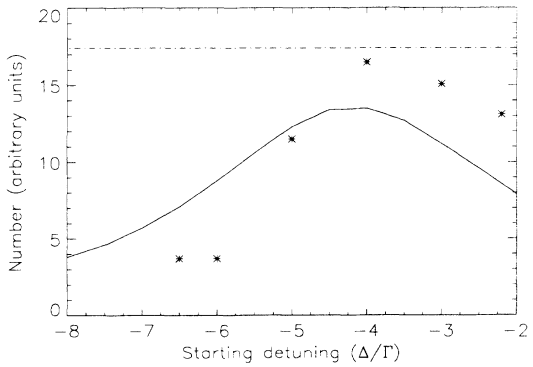

FIG. 7. The solid line shows the model's predictions for the number of trapped atoms when the laser's frequency is linearly chirped. The abscissa shows the starting frequency of the chirp cycle. Each chirp cycle stopped at -1.0Γ detuning, and the cycles repeated every 1.0 ms. The simulation used a beam size of 2.0 cm and an intensity of 1.6 mW/cm^2. The dashed line represents the number of atoms predicted for the case of no chirp and the optimum detuning of -3Γ. The asterisks show our measurements at the same conditions.

When the chirp is started at a detuning larger than -4Γ, the number of atoms observed is lower than predicted by the model. We believe that this is because hyperfine-changing collisions [5] during the far-detuned parts of the chirp cycle increase the loss rate of the trap. We tested this hypothesis by measuring the trap's characteristic decay times after the trapping laser detuning was rapidly shifted. The rate at which atoms left the trap was more than twice as large at -4Γ than at -2.5Γ, and continued to increase with larger detuning, thus supporting this hypothesis.

We tried another proposed [14] method for improving the capture rate: using broadband trapping light, or light with several closely spaced frequency components. This technique also did not work as well as a single fixed frequency. Recent theoretical work by Parkins and Zoller [24,25] provides a plausible explanation for these results. They have shown that low-velocity atoms experience heating rather than cooling under conditions similar to those used in the experiment. Our results are consistent with those of other unsuccessful attempts to increase the number of trapped atoms by frequency chirping [15] or trapping with broadband light [15,26], and it is now clear why these techniques fail.

VI. DENSITY OF THE TRAPPED ATOMS

As a final study, we have measured the dependence of the density of atoms in the trap on the trap parameters. We have observed a number of trends, but are unable to model the density quantitatively because of its complex dependence on radiation-trapping forces [19]. An additional complication in the interpretation is that the absolute measurement of the density could vary by as much as 25%.

First, we see the density increase with increasing magnetic-field gradient (Fig. 8). Second, the density increases with increasing detuning of the trapping lasers (Fig. 9). Third, the density increases with increasing intensity of the laser beams (this effect tapers off at high intensities). Finally, there is little if any dependence of the density of atoms in the trap on the diameter of the trapping beams (in contrast with our observations of the number of atoms).

Some of these trends can be explained qualitatively with the radiation-trapping density model of Ref. [19]. This model gives a density limit due to the balance of trapping, absorption, and radiation-trapping forces:

$$n_{\max} \sim \frac{ck}{\sigma_r(\sigma_r - \sigma_l)I} , \tag{7}$$

where I is the incident intensity, k is the spring constant, σ_l and σ_r are the cross sections for absorption of incident laser and scattered light, and c is the speed of light. The $(\sigma_r$-$\sigma_l)$ difference depends on the overlap between the reemission spectrum for scattered laser light and the absorption spectrum in a strong standing-wave field. As

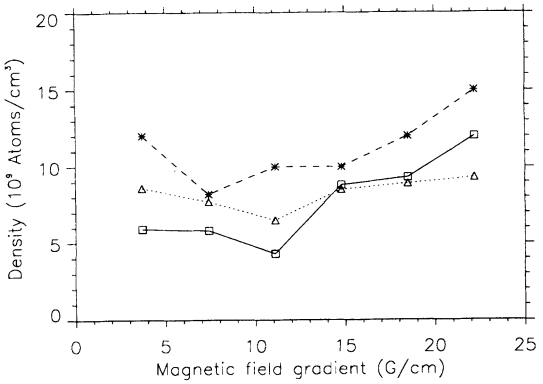

FIG. 8. The number density of trapped atoms vs magnetic-field gradient. Three different trap-laser detunings are shown: -1Γ (squares), -1.5Γ (triangles), and -2.5Γ (asterisks). The beam diameter was 1.4 cm and the intensity was 3.6 mW/cm^2 per beam. The symbols are our experimental data; the connecting lines are only to guide the eye. The field gradients shown on the abscissa are along the symmetry axis of the pair of field coils. Gradients in the other two dimensions are half of this.

discussed in Ref. [19], this difference is quite difficult to calculate accurately for a real cesium atom in three dimensions. The spring constant in Eq. (7) is

$$k \sim \frac{\frac{dB}{dz}\Delta\beta}{\left[1+\beta+\left[\frac{\Delta}{\Gamma}\right]^2\right]^2}, \tag{8}$$

where dB/dz is the magnetic-field gradient along the axis of the coils. From Eqs. (7) and (8) one would expect the qualitative dependencies on intensity and field gradient

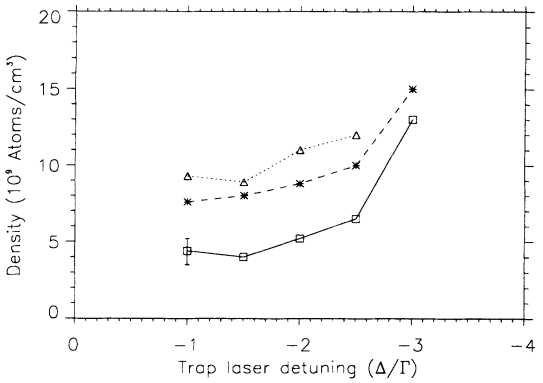

FIG. 9. Variation of the number density of trapped atoms with detuning of the trap laser. Three beam sizes were used, all with approximately 5 mW per beam, to give the three curves at 1.6 mW/cm^2 (squares), 3.6 mW/cm^2 (triangles), and 9 mW/cm^2 (asterisks). The magnetic-field gradient was held constant at 16 G/cm. The symbols show our experimental data; the connecting lines are only to guide the eye. A characteristic error bar, determined from scatter in the values obtained in repeated trials, is shown for one point. As the detuning was increased beyond -2.5Γ, the number of trapped atoms dropped precipitously.

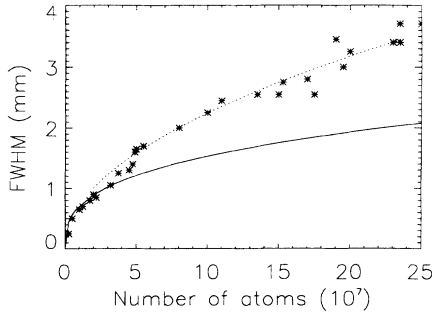

FIG. 10. The data of Sesko *et al.* [19] (asterisks) for the diameter of the cloud of trapped atoms vs the number of atoms in the trap. The solid line represents the prediction of Eq. (7) ($L \sim N^{1/3}$). The dotted line shows the same prediction with the added constraint that the optical thickness cannot become so large that an average reemitted photon will scatter more than once in escaping the cloud.

that are observed. The detuning dependence is too complex to predict.

On a final note, our data show that, in general, large clouds ($N > 3\times10^7$ atoms) have lower densities than small clouds. This is consistent with the data of Sesko *et al.* [19], and inconsistent with Eq. (7). We believe that the source of this discrepancy is the fact that Eq. (7) was derived with the assumption that the photons are scattered no more than twice. However, with more than 3×10^7 atoms and the density predicted by Eq. (7), the optical thickness would be large enough for a significant number of photons to scatter more than twice in the cloud of trapped atoms before escaping. This would increase the radiation-trapping force, causing the cloud to expand and the density to drop below the value given by Eq. (7). If the cloud expands too far, however, the optical thickness will begin to decrease, thereby reducing the radiation-trapping force. This leads to a balance of forces that maintains the density of a large cloud at an optical thickness where, on the average, each photon absorbed from the laser beam will, after reemission, scatter no more than once on its way out of the cloud. This means that when the number of atoms is greater than 3×10^7 the diameter of the cloud will go as the square root of the number of atoms in the cloud rather than as the cube root as Eq. (7) predicts. In Fig. 10 we show that this dependence is very close to what was reported in Ref. [19]. Our current data are similar but cover a smaller range.

VII. CONCLUSION

We have reported results of a study of optical trapping in a vapor-cell Zeeman optical trap. We have developed a model that agrees with our observations of how the number of atoms in the trap varies with the intensity of the trapping beams, the size of the trapping beams, the detuning of the laser, and the strength of the magnetic field. Our model includes the one-dimensional slowing force on an atom moving through the trap, and the three-dimensional effects of the magnetic field. We are

confident that we can accurately predict numbers of atoms for any reasonable trap parameters. In addition, we have shown that for many conditions it is possible to reliably calculate dependences using a simple one-dimensional, two-level model that neglects the magnetic field. This allows one to estimate the capture rates and numbers of trapped atoms quite easily. Attempts to increase the number of trapped atoms by frequency chirping or by bandwidth broadening the laser were not successful, and we can now explain why these techniques do not work. Finally, we have described the results of measurements of the trap density as a function of the trap parameters. We observed small increases in density with magnetic field, laser intensity, and detuning.

ACKNOWLEDGMENTS

This work was supported by the office of Naval Research and the National Science Foundation. We would like to thank E. Cornell and C. Monroe for useful discussions. We are also grateful to K. E. Gibble, S. Kasapi, and S. Chu for providing us with their data prior to publication, and for permission to reproduce it.

[1] J. Opt. Soc. Am. B **6** (22) (1989) Special Issue on laser cooling and trapping.
[2] D. Grison, B. Lounis, C. Salomon, J. Y. Courtois, and G. Grynberg, Europhys. Lett. **15**, 149 (1991).
[3] J. W. R. Tabosa, G. Chen, Z. Hu, R. B. Lee, and H. J. Kimble, Phys. Rev. Lett. **66**, 3245 (1991).
[4] A. Gallagher and D. Pritchard, Phys. Rev. Lett. **63**, 957 (1989).
[5] D. Sesko, T. Walker, C. Monroe, A. Gallagher, and C. Wieman, Phys. Rev. Lett. **63**, 961 (1989).
[6] P. D. Lett, P. S. Jessen, W. D. Phillips, S. L. Rolston, C. I. Westbrook, and P. L. Gould, Phys. Rev. Lett. **67**, 2139 (1991).
[7] P. S. Julienne and J. Vigue, Phys. Rev. A **44**, 4464 (1991).
[8] C. Monroe, H. Robinson, and C. Wieman, Opt. Lett. **16**, 50 (1991).
[9] S. L. Rolston and W. D. Phillips, Proc. IEEE **79**, 943 (1991).
[10] S. Freedman and K. Coulter (private communication).
[11] C. Wieman, C. Monroe, and E. Cornell, in *Tenth-International Conference on Laser Spectroscopy,* edited by M. Ducloy, E. Giacobino, and G. Camy (World Scientific, Singapore, 1992), p. 77.
[12] E. Cornell, C. Monroe, and C. Wieman, Phys. Rev. Lett. **67**, 2439 (1991).
[13] This idea has been suggested by many people. The first, to our knowledge, was D. Pritchard in about 1985. Also see Ref. [15].
[14] M. Zhu, C. W. Oates, and J. L. Hall, Phys. Rev. Lett. **67**, 46 (1991).
[15] K. E. Gibble, S. Kasapi, and S. Chu, Opt. Lett. **17**, 526 (1992).
[16] C. Monroe, W. Swann, H. Robinson, and C. Wieman, Phys. Rev. Lett. **65**, 1571 (1990).
[17] E. L. Raab, M. Prentiss, A. Cable, S. Chu, and D. Pritchard, Phys. Rev. Lett. **59**, 2631 (1987).
[18] C. Wieman and L. Hollberg, Rev. Sci. Instrum. **62**, 1 (1991).
[19] D. W. Sesko, T. G. Walker, and C. E. Wieman, J. Opt. Soc. Am. B **8**, 946 (1991); T. G. Walker, D. W. Sesko, and C. E. Wieman, Phys. Rev. Lett. **64**, 408 (1990).
[20] E. Cornell, C. Monroe, and C. Wieman (unpublished).
[21] H. Metcalf, J. Opt. Soc. Am. B **6**, 2206 (1989).
[22] R. N. Watts and C. E. Wieman, Opt. Lett. **11**, 291 (1986).
[23] W. Ertmer, R. Blatt, J. L. Hall, and M. Zhu, Phys. Rev. Lett. **54**, 996 (1985).
[24] A. S. Parkins and P. Zoller, Phys. Rev. A **45**, R6161 (1992).
[25] A. S. Parkins and P. Zoller, Phys. Rev. A **45**, 6522 (1992).
[26] M. Zhu and J. L. Hall (private communication).

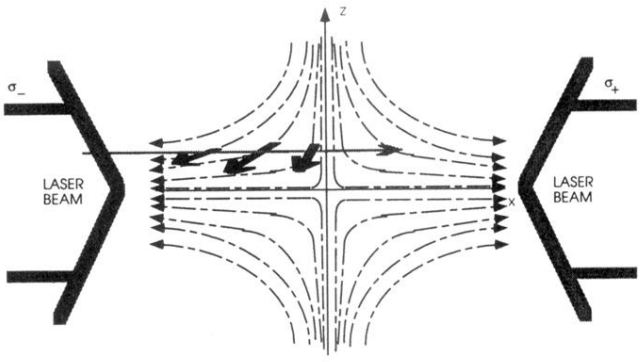

FIG. 5. Spatial variation of the magnetic field in the trap. The grey arrow shows one possible path of an atom through the trap. The dark, black arrows indicate the direction of the magnetic field at several points along the atom's path.